RSC Advances

ROYAL SOCIETY OF CHEMISTRY

www.rsc.org/advances

RSC Advances

RSCPublishing

paper

A D–π–A–π–A type dye for highly efficient dye-sensitized solar cells

Cite this: DOI: 10.1039/xoxxoooooox

Chao-Feng Du,[ab*] Lei Jiang,[b*] Lei Sun,[b] Nian-Yu Huang[a] and Wei-Qiao Deng[b†]

Received ooth xxxx 2015,
Accepted ooth xxxx 2015

DOI: 10.1039/xoxxoooooox

www.rsc.org/

We synthesized a D–π–A–π–A type dye and demonstrated its application in dye-sensitized solar cells (DSSCs). This D–π–A–π–A type dye, named as C321, was consisted of a triphenylamine as a donor, a 3,4-ethylenedioxythiophene (EDOT) as a π-bridge, and a benzothiazole (BTDA)–phenyl-cyanoacrylic acid as an A–π–A group. Comparing with DSSCs based on a traditional D–π–A type dye C311, the DSSCs based on C321 exhibited a significant enhancement of cell performances. A power conversion efficiency of 8.2% was achieved for DSSCs based on C321, which was 9 times higher than that for DSSCs based on C311 (0.9%). The theoretical calculations and electrochemical impedance spectroscopy investigations revealed the mechanism of the enhancement of cell performances.

1. Introduction

Dye sensitized solar cells (DSSCs) are regarded as the promising devices for high-efficiency and low-cost solar energy conversion, since O'Regan and Grätzel reported the first DSSC in 1991. [1-4] Small cells have recently been achieved with an efficiency of over 13.0%[1-5] and a lifetime of more than 1000 hours. [6] The further development of DSSCs relies on the discovery of new dyes that provide better photovoltaic properties. Explorations of new dyes for DSSCs can be divided into two categories: 1) metal complex dyes with transition metal such as N3, [7,8] black dye, [9-11] YD2-*o*-C8 [12] and SM315; [5] 2) metal-free organic dyes such as C218, [13,14] C219 [15] and D5.[16,17] Comparing with the metal complex dyes, the metal-free organic dyes are much easier to tune their absorption spectral and electrochemical properties through tailoring molecules. [18]

Generally, metal-free organic dyes are consisted of a donor-π-acceptor (D-π-A) type structure, of which D is an electron-donating unit, A is an electron-accepting unit and π is a π-conjugated spacer unit. The D-π-A dye structure can induce intramolecular charge transfer (ICT) from donor to acceptor group which facilitates the high molar extinction coefficient and redshift the absorption of dye molecules. By changing donor, acceptor or π-spacer groups, the energy levels of the highest occupied molecular orbital (HOMO) and the lowest unoccupied molecular orbital (LUMO) can be shifted, resulting in various physical and chemical properties of dye molecules. [19] The most common D-π-A type dyes were consisted of a triphenylamine group as donor, a cyanoacetic acid group as acceptor,and a thiophene (T) and its derivatives as π -spacer. [15,20-26] For example, the cell based on dye C219 exhibited a power conversion efficiency (PCE) – 10.3%, which has been near the created by ruthenium (II) complex dyes. [15] To improve the PCE of metal-free organic dyes, a strategy is to introduce an electron-accepting unit into the π-spacer group which can be named as a D-π-A-A type structure. [23,27-29] For example, the introduction of benzothiadiazole (BTDA) unit, an acceptor group, into the π-spacer group can reduce the gap between HOMO and LUMO significantly, which results in an improved PCE. However, some D-π-A-A type dyes may not be efficient since the electron recombination between adjacent acceptor groups and TiO2 substrate can be intensified. [30]

Here, we proposed a D-π-A-π-A type dye by introducing a π group into a D-π-A-A type dye for DSSCs. As an example, we synthesized a dye C321 consisted of a triphenylamine as a donor, a 3,4-ethylenedioxythiophene (EDOT) as a π-bridge, and a benzothiazole (BTDA)–phenyl-cyanoacrylic acid as a A–π–A group, as shown in Scheme 1. The PCE of DSSCs based on C321 can reach as high as 8.3%, which is 9 times higher than that of DSSCs based on a traditional D-π-A type dye C311. Both theoretical and experimental results indicated that the enhancement of PCE may origin from the improvement of the recombination process in DSSCs.

2. Results and discussion

2.1. Synthesis

Compound 4 (4-Bromo-7-(4-formylphenyl)-2,1,3-benzothiadiazole) was synthesized via a Suzuki-Miyaura coupling reaction. Compounds 9, 11 and 12 were synthesized via Still coupling reactions. The synthetic routes of C311 and C321 are

[a] *Hubei Key Laboratory of Natural Products Research and Development, College of Chemistry and Life Sciences, China Three Gorges University, Yichang 443002, China.*
[b] *State Key Laboratory of Molecular Reaction Dynamics, Dalian National Laboratory for Clean Energy, Dalian Institute of Chemical Physics, Chinese Academy of Sciences, Dalian 116023, China. E-mail: dengwq@dicp.ac.cn*
* These authors contributed equally to this work

† Electronic Supplementary Information (ESI) available: [Additional experimental data] See DOI: 10.1039/b000000x/

shown in Scheme 1 and the detailed synthesis procedures of 1 to 12 are described in the Supporting Information.

2.2. Theoretical Calculations

The electronic configurations of the isolated dyes were examined by using B3LYP [33] /6-311G** hybrid functional implanted in a Gaussian09 software. [35] For calculating the absorption spectrum in CH3CN solution, a time-dependent density functional theoretical (TDDFT) with the MPW1K [34] functional was employed. The optimized geometries of the two dyes, as shown in Figure 1, have

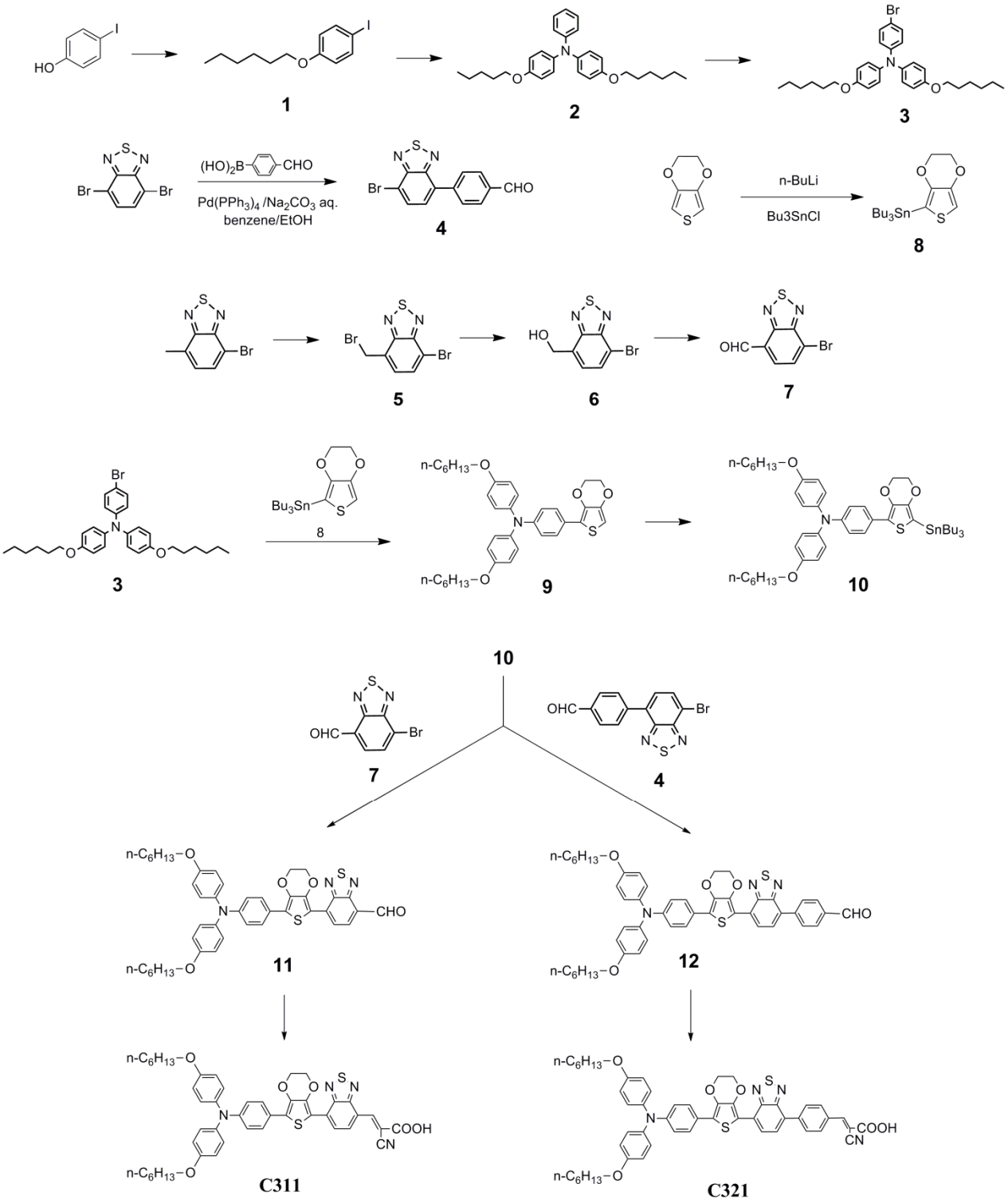

Scheme 1. Synthesis of dyes **C311**and **C321**.

planar structures in the ground state. The calculated electron-density diagrams of HOMOs and LUMOs were shown in Figure 1 as well. In both dyes, the HOMOs and LUMOs exhibit π-character. While the HOMO is mainly localized over the donor groups, the LUMO is localized on the accepter and π-spacer groups. The localizations of molecular orbitals are expected to have an intramolecular charge separation upon excitation. The calculated dipole-allowed absorptions were listed in Table 1. The strong absorption peaks for each dye arise from S0 → S1, which correspond to the promotion of an electron from the HOMO to LUMO. Therefore, the lowest-lying absorption transitions were all assigned to π → π* type transitions from donor to acceptor moieties through a π-spacer. Comparing with C321, C311 exhibited a maximum absorption at longer wavelength 610 nm and similar oscillator strength of absorption peak, which probably results in the greater overlap between its absorption spectrum and the solar spectrum. For these two dyes, the wavelengths of maximum absorption peaks decreased with the additional phenyl group about 50 nm. Just based on the calculated absorption spectral, the D–π–A–π–A type dye C321 should have a weaker light adsorption than the D–π–A type dye C311.

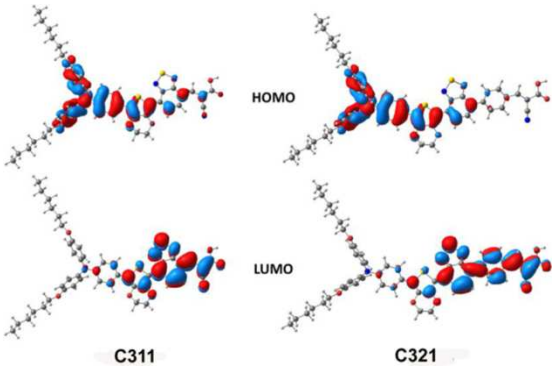

Figure 1. HOMO and LUMO electron density distributions for frontier orbitals of dyes C311 and C321.

The electronic coupling strength governing the photoinduced electron transfer is probably determined by the interaction between the LUMO orbital of dye and the conduction band of TiO2. To investigate this interaction, a detailed investigation of the partial density of state (PDOS) of the adsorbate's LUMO has been made. The dye-absorbed geometries were optimized in the gas phase using the Dmol3 package and the electronic structure of the combined system was subsequently calculated at B3LYP/SVP level using the Gaussian09 software. The injection times for C311 and C321 are 17 and 12 fs, respectively. The electron injection efficiency is calculated by: ηinj = 1 – τinj/τlifetime. For organic dyes, the injection process is in competition with singlet state decay to ground (singlet excited state lifetime ranging from ~ 100 ps to a few nanoseconds), requiring τinj < 10ps to achieve an injection efficiency of 90% or even more. If the excited state lifetime is set to 1ps for C311 and C321, their ηinj equal to 98% and 99%, respectively. The calculated injection times indicated these dyes exhibit strong electronic coupling with TiO2 cluster and great quantum yield for electron injection. The calculated injection efficiencies for all dyes were very close to 100%. It indicates that the introduction of BTDA, electron-accepting unit, close to cyanoacetic acid group will not affect the electron injection process from dye to TiO2 substrate.

Table 1. The calculated dipole-allowed lowest lying transition for **C311** and **C321** under the TD-MPW1K

	Transition	Wavelength (nm)	Oscillator Strength	Major Contributions
C311	$S_0 \rightarrow S_1$	610	1.3452	HOMO → LUMO (88%)
C321	$S_0 \rightarrow S_1$	553	1.3824	HOMO → LUMO (78%)

To reduce the charge recombination rate between the dye cation and the injected electron, the positive charge localized primarily on the donor group should be farther away from the electrode surface. Based on nonadiabatic electron-transfer theory, the recombination rate can be analyzed in terms of the Marcus formula, where H_{AB}^2 is the electronic coupling between the donor and acceptor groups, ΔG^0 is the reaction free energy, and λ is the reorganization energy. The term H_{AB}^2 can be represented in terms of an exponential function of the spatial separation r between the donor and acceptor groups. [31,32] According to the work by Clifford et al., [31] ΔG^0 is approximately equal to λ in the recombination dynamics, and r is the primary factor affecting the recombination rate. Here, r is approximated by using the HOMO barycenter (r_{HOMO}) of the neutral dye. Based on the geometries of dye-TiO_2 complexes, the values of r_{HOMO} of the isolated dye molecule on TiO_2 substrate were evaluated as 1.69 and 2.15 nm for **C311** and **C321**, respectively. The spatial separation between HOMO and TiO_2 substrate increased obviously after the phenyl group was introduced. It indicates that the phenyl group can suppress the electron recombination between dye and TiO_2 significantly, which may result in an enhancement of the photocurrent of DSSCs based on **C321**.

$$k_{re} = \frac{H_{AB}^{\ 2}}{\sqrt{4\pi\lambda k_B T}} \exp\left(-\frac{\left(\Delta G^0 - \lambda\right)^2}{4\lambda k_B T}\right) \qquad (1)$$

Based on the quantum chemical calculations, we studied the optical properties, electron injection time and electron recombination for **C311** and **C321**. The results showed that although **C311** has a promising absorption spectral performance, **C321** exhibits a weak electron recombination process that may lead to a high photocurrent.

2.3. Spectroscopic properties

The UV-vis absorption spectra of **C311** and **C321** measured in dilute chlorobenzene solution were shown in Figure 2, exhibiting two absorption bands over a range of 350-800 nm. The bands at 378 nm of **C311** and 364 nm of **C321** corresponded to the π–π* transition of the conjugated system. The longest wavelength absorption peak of **C321** (λ_{max} = 511 nm) was assigned to a charge-

Table 2. Calculated and experimental parameters for dyes **C311** and **C321**.

Dye	$\lambda_{max,Exp}$ (nm)	$\varepsilon_{max,\ Exp}$ ($M^{-1}cm^{-1}$)	E_{ox} (V)	E_{red} (V)	$HOMO^{exp}$ (eV)	$LUMO^{exp}$ (eV)	$HOMO^{Cal}$ (eV)	$LUMO^{Cal}$ (eV)	E_g^{opt} (eV)	E_g^{Cal} (eV)
C311	563	4.11×10^4	0.7	-0.95	-4.89	-3.24	-4.95	-3.12	1.65	1.83
C321	511	4.35×10^4	0.65	-1.2	-4.84	-2.99	-4.82	-2.94	1.85	1.92

transfer (CT) transition. The CT band of **C311** (λ_{max} = 563 nm) was significantly red-shifted compared to that of **C321**. Our calculation results showed that the longest wavelength absorption peaks of **C311** and **C321** were 610 and 553nm, respectively, which were in good agreement with the experimental values. The molar extinction coefficient for the CT transition of **C311** and **C321** were 4.11×10^4 and 4.35×10^4 M^{-1} cm^{-1}, respectively, which are much higher than that of the well-known dye N719 ($<2 \times 10^4$ M^{-1} cm^{-1}). The UV-vis spectra of **C311** and **C321** adsorbed onto 2 μm transparent TiO_2 films (Figure 2b) showed a significant red-shift of the CT-band for **C321** (λ_{max} shifted from 511 nm to 531 nm) and a slight red-shift for **C311** (λ_{max} shifted from 563 to 566 nm) compared to their spectra in solution. All data were listed in Table 2.

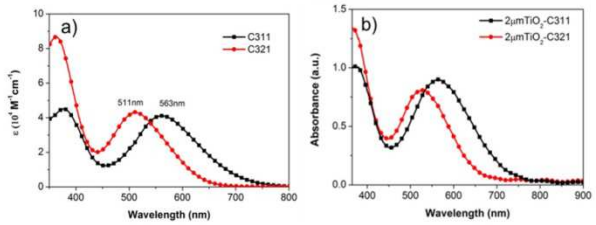

Figure 2. a) UV-vis spectra of dyes **C311** and **C321** in chlorobenzene. b) UV-vis spectra of dyes **C311** and **C321** on transparent TiO_2 films (2 μm).

2.4. Electrochemical properties

To evaluate the energetics of **C311** and **C321**, cyclic voltammograms (CV) was performed to measure the oxidation potentials (E_{ox}), which correspond to the HOMO level potentials of the sensitizers. The oxidation potentials of the dyes were measured in dichloromethane containing 0.1M tetrabutylammonium hexafluorophosphate (TBAHFP) as electrolyte, ferrocene/ferrocenium (Fc/Fc^+) as an internal reference (Figure 3). The results were summarized in Table 2, the half-wave potentials

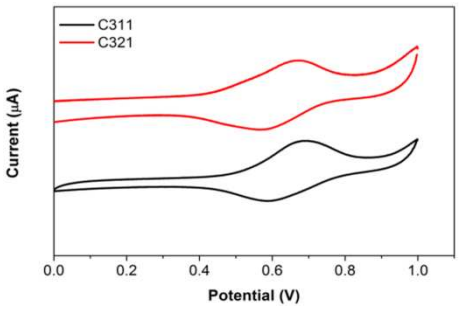

Figure 3. CV spectra of **C311** and **C321** in dichloromethane (CH_2Cl_2) solution (5×10^{-4} M) containing 0.1 M TBAHFP.

of **C311** and **C321** were 0.5 and 0.45 V, respectively. The HOMO levels of **C311** and **C321** can be determined as -4.89 eV and -4.84 eV vs. vacuum, respectively. The LUMO level can be estimated from the values of oxidation potential and the zero-to-zero transition energy measured at the intersection of absorption spectra. We estimated that the LUMO energy levels of **C311** and **C321** were -3.24 eV and -2.99 eV, respectively, which lie above the conduction band edge of TiO_2 (approximately -4.0 eV vs. vacuum). This result indicated that the driving force is sufficient for electron injecting from the dyes into the conduction band of TiO_2. The energies of HOMO and LUMO of the dyes were in good agreement with the calculation results (list in table 2).

2.5. Application in DSSCs

The current–voltage (*J–V*) characteristics of DSSCs based on **C311** and **C321** on 6 μm thick TiO_2 films (with 5 μm scattering) employing a I^-/I_3^- electrolyte were measured under one sun solar illumination conditions (AM 1.5G, 100 mW cm^{-2}), as shown in Figure 4. The electrolyte solution was consisted of 1.0 M 1,3-dimethylimidazolium iodide, 0.05 M lithium iodide (LiI), 0.03 M iodine, 0.5 M tert-butylpyridine and 0.1 M guanidinium thiocyanate in an 85:15 (v/v) acetonitrile/valeronitrile mixture (E1). The photovoltaic parameters of DSSCs including short-circuit photocurrent density (J_{sc}), open-circuit photovoltage (V_{oc}), fill factor (*FF*), and solar-to-electric power conversion efficiencies (η) were summarized in Table 3. The DSSCs based on **C321** provided an overall solar-to-electric power conversion efficiency of 8.2% with a high short-circuit photocurrent density 16.78 mA/cm^2 and a high open-circuit photovoltage 686 mV (*FF* = 71.1%). Under the same conditions, the cells based on **C311** showed a poor performance with an overall η of 0.9% due to low J_{sc} and V_{oc} values (J_{sc} = 2.32 mA/cm^2, V_{oc} = 572 mV, *FF* = 70.6%). The incident photon-to-current conversion efficiency (IPCE) spectra of DSSCs based on **C321** and **C311** were much different, as shown in Figure 5. The IPCE of cells based on **C321** exhibited 89% at 560 nm, while cells based on **C311** show only 14% at 540 nm. The photovoltaic performances of DSSCs have been optimized by using different TiO_2 film thickness (Figure S1, Table 4). A TiO_2 layer (6 μm transparent + 5 μm scattering) showed the best photocurrent density and solar-to-electric power conversion efficiencies.

Table 3. Photovoltaic parameters of DSSCs sensitized by **C311** and **C321**.

Dye	J_{sc} (mAcm^{-2})	V_{oc} (mV)	*FF* (%)	η (%)
C311	2.32	572	70.6	0.9
C321	16.78	686	71.1	8.2

The difference between **C311** and **C321** is only a π-conjugated spacer unit (phenyl ring) between the benzothiadiazole unit and the

anchoring group. However, this small modification changed the D–π–A type dye **C311** as the D–π–A–π–A type dye **C321,** which results in a significant enhancement of the photovoltaic performances. In order to explain this phenomenon, the electrochemical impedance spectroscopy (EIS) of as-prepared DSSCs based on **C311** and **C321** were measured. Figure 6 shows

Table 4. Photovoltaic parameters of DSSCs sensitized by **C321** dye absorbed on TiO_2 films of different thicknesses.

entry	TiO_2 film thickness (μm)	J_{sc} ($mAcm^{-2}$)	V_{oc} (mV)	*FF* (%)	η (%)
1	4+5	12.91	678	71.7	6.3
2	6+5	16.44	688	71.2	8.1
3	8+5	14.46	684	74.2	7.3

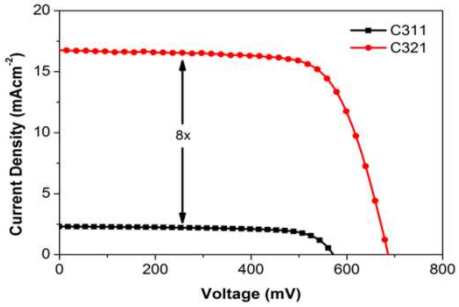

Figure 4. *J-V* curves of DSSCs sensitized with **C311** and **C321**.

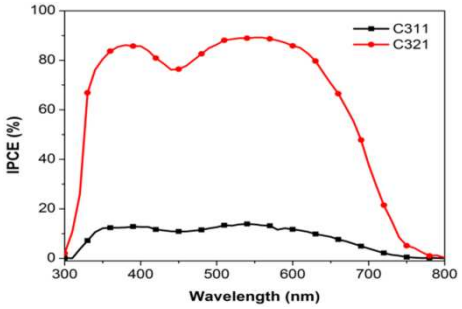

Figure 5. IPCE spectra for DSSCs sensitized with **C311** and **C321**.

the Nyquist and Bode plots for DSSCs based on **C311** and **C321**. The responses in the frequency regions around 10^3~10^5, 10~10^2, and 0.05 to 1 Hz were contributed to charge-transfer processes occurring at the Pt electrode/electrolyte interface, the TiO_2 electrode/dye/electrolyte interface, and the Nernst diffusion within the electrolyte, respectively. [36] The larger semicircle in the Nyquist plots was attributed to the charge-transfer resistance (R_{ct}) at the TiO_2 electrode/dye/electrolyte interface. The R_{ct} values can be calculated by fitting the curves using an equivalent model, [37] the equivalent circuit shown in figure S2. The fitted R_{ct} of the cells sensitized by C311 and C321 are 9.7 and 42.6 Ω. It corresponds to the charge recombination rate (k_r) at the TiO_2/dye/electrolyte interface of DSSCs. Through the recombination rate and R_{ct} equation, [38] where A is the cell area, T is the temperature, k_B is Boltzmann's constant, L is the thickness of the film, q is elementary charge and n_c is the density of electrons in the conduction band, the charge-transfer resistance is inversely proportional to the recombination rate.

$$k_r = \frac{k_B T}{R_{ct} A L q^2 n_c} \qquad (2)$$

The n_c values can be calculated by the by fitting the curves of Nyquist phase (Equation S1). The n_c values of the cells sensitized by **C311** and **C321** are 3.72×10^{17} and 1.28×10^{19} cm^{-3}, respectively. Through the above equation, the k_r of DSSCs sensitized by **C311** and **C321** are 142.6 and 4.2 s^{-1}. The recombination rate of **C311** is 34 times higher than that of **C321**, demonstrating that the charge recombination of the device sensitized by **C321** is efficiently suppressed, leading to the improvement of the photocurrent and photovoltaic. The electron lifetime (t_n) can be estimated according to the equation: $t_n = 1/(2\pi f_{max})$, where f_{max} is the maximum frequency of the mid-frequency peak. [39] The f_{max} values were determined as 2511 and 39.8 Hz for the DSSCs based on **C311** and **C321**, respectively. Correspondingly, the calculated electron lifetimes were 0.13 and 4.0 ms for the DSSCs based on **C311** and **C321**. This result suggests that the t_n of the DSSCs based on **C321** exhibited a 123 times higher than that of DSSCs based on **C311**, leading to the improvement of the photocurrent. This experimental result was in consistent with the calculation result that **C321** has a much weaker recombination process than **C311**. The EIS results explained the significant enhancement of cell performance by replacing a D–π–A type dye (**C311**) with a D–π–A–π–A type dye (**C321**).

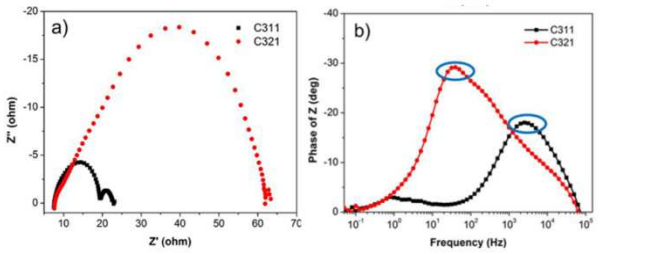

Figure 6. (a) Nyquist and (b) Bode phase plots of dye-sensitized solar cells sensitized by C311 and C321 dyes. The cells were measured at 0.7 V bias voltage in the dark.

3. Conclusion

In summary, we report a new D–π–A–π–A type dye **C321**. Due to the introduction of a π-conjugated spacer unit (phenyl ring) between the benzothiadiazole (BTDA) unit and the anchoring group, **C321** exhibited a great enhancement on the photovoltaic performance compared with the traditional D–π–A type dye **C311**. The cell efficiency of DSSCs based on **C321** can reach as high as 8.2%, which was superior to that of DSSCs based on **C311** (0.9%) under one sun illumination. The EIS results revealed that **C321** has a higher charge-transfer resistance (R_{ct}) and a higher electron

lifetime than **C311** in DSSCs, which was in consistent with the calculation results. These results suggested that the D–π–A–π–A type dye would be a novel class of dyes for efficient DSSCs.

4. Experimental Section

4.1. Device fabrication

The photoelectrodes were preapared by screen-printing double layers of nanocrystalline TiO_2 particles, for transparent films a 6-μm thick layer of 20 nm-sized TiO_2 particles was printed on the fluorine doped tin oxide (FTO, TCO-15, 14ohm/square, NSG, Japan) conducting glass by successive screen printing using a TiO_2 paste (DSL 18-NR, Dyesol, Australia). Where applicable, a 5-μm thick scattering layer of 400 nm sized TiO_2 particles (WER-2, Dyesol, Australia) was then covered on top of the transparent layer. The electrodes were dried at 150 ºC for 5 min and then heated at 500 ºC for 45 min, after cooling to room temperature the electrodes were soaked in a 40 mM $TiCl_4$ aqueous solution at 70 ºC for 40 min. After sintering at 500 ºC for 15 min and cooling to 100 ºC, the sintered elcctrodes were immersed into sensitizer solution (0.3 mM of the dye with 2 mM of chenodeoxycholic acid, in chlorobenzene) for 6h, and then assembled using a thermally platinized FTO counter electrode through a 50 μm thick hot melt ring (Bynel, Dupont) by heating. The electrolyte solution was 1.0 M 1,3-dimethylimidazolium iodide, 0.05 M lithium iodide (LiI), 0.03 M iodine, 0.5 M tert-butylpyridine and 0.1 M guanidinium thiocyanate in an 85:15 (v/v) acetonitrile/valeronitrile mixture. The electrolyte was filled in the cell's internal space by using a vacuum pump.

4.2. Device characterization

The UV-Vis absorption spectrum was recorded on a Persee TU-1810 UV-Vis spectrometer. Sun 2000 solar simulator (Abet-technologies, USA) was used to give an irradiance of 100 mW cm^{-2} (AM 1.5 G) of the cell and and light intensity was measured by using a silicon reference cell. The photocurrent density-voltage (*J-V*) characteristics under simulated AM 1.5G illumination were measured by using a Keithley 2400 Source meter. Incident photon-to-current conversion efficiency (IPCE) were measured by a QE/IPCE Measurement Kit (Oriel, USA, M66901), and the incident-photon flux was obtained by using a calibrated silicon reference photodiode. The devices were masked to a working area of 0.160 cm^2. Electrochemical data was obtained by a Versa STAT 3 (METEK, USA) electrochemical workstation.

4.3. Synthesis of photosensitzres

All reagents were purchased from Aladdin, TCI and Alfa Aesar and used as received without further purification. The solvents were purified by distillation under a nitrogen atmosphere prior to use. 1H NMR and 13C NMR spectra were recorded on a BRUKER AVANCE 400 MHz NMR Instrument by using CDCl3 and DMSO-d6 as solvent, using tetramethylsilane as an internal reference. MALDI-TOF was performed on an AB SCIEX instrument, using CHCA as a matrix.

2-Cyano-3-{7-{4-[N,N-Bis(4-hexyloxyphenyl)-4-aminophenyl] -3,4-ethylenedioxythiophene-2-yl}benzo[1,2,5]thiadiazole-4-yl} acrylic acid (C311): Compound 11 (150 mg, 0.21 mmol), ammonium acetate (16 mg, 0.21 mmol) and cyanoacetic acid (179 mg, 2.2 mmol) were dissolved in a mixture of DCM/MeCN (60 mL, 2:1 v/v). The mixture was refluxed under argon atmosphere for 10h. After cooling to room temperature, the reaction mixture was dissolved in dichloromethane (3 ×50 mL), washed with water (2 × 20 mL) and dried over $MgSO_4$. The solvent was removed in vacuo. The crude product was purified by column chromatography (dichloromethane/methanol) to obtain dye **C311** as a dark blue solid (111 mg, 65%). ^{1}H NMR (400 MHz, $CDCl_3$) δ: 9.26(s, 1H), 8.92(d, J = 7.6Hz, 1H), 8.59(d, J = 7.6Hz, 1H), 7.69(d, J = 8.4Hz, 2H), 7.08(d, J = 8.4Hz, 4H), 6.95(d, J = 8.4Hz, 2H), 6.85(d, J = 8.8Hz, 4H), 4.52(m, 2H), 4.42(m, 2H), 3.96(t, J = 6.0Hz, 4H), 1.82(m, 4H), 1.51(m, 4H), 1.37(m, 8H), 0.94(m, 6H). ^{13}C NMR (400 MHz, DMSO-d_6) δ: 155.4, 153.9, 150.7, 147.7, 142.8, 139.8, 139.5, 137.3, 128.1, 127.2, 126.8, 126.7, 124.4, 123.8, 122.7, 121.0, 119.1, 115.5, 108.9, 67.6, 65.1, 64.2, 30.9, 28.7, 25.2, 22.0, 13.8. MALDI-TOF (m/z): 814.6 [M^+].

3-{4-{7-{4-[N,N-Bis(4-hexyloxyphenyl)-4-aminophenyl]-3,4-ethylenedioxythiophene-2-yl}benzo[1,2,5]thiadiazole-4-yl} phenyl }-2-cyanoacrylic acid (C321): Dye **C321** was synthesized by the same method as dye **C311** by using compound 12 (85 mg, 0.10 mmol) instead of compound 11. Dye **C321** was obtained as a dark blue solid (41 mg, 45%). ^{1}H NMR (400 MHz, DMSO-d_6) δ: 8.51(d, J = 8.0Hz, 1H), 8.18(d, J = 8.4Hz, 2H), 8.05(m, 4H), 7.61(d, J = 8.8Hz, 2H), 7.03(d, J = 8.8Hz, 4H), 6.92(d, J = 8.8Hz, 4H), 6.84(d, J = 8.8Hz, 2H), 4.52(m, 2H), 4.42(m, 2H), 3.95(t, J = 6.4Hz, 4H), 1.74(m, 4H), 1.45(m, 4H), 1.33(m, 8H), 0.90(m, 6H). ^{13}C NMR (400 MHz, DMSO-d_6) δ: 155.8, 153.3, 152.3, 147.9, 142.4, 140.1, 137.8, 129.9, 129.7, 127.3, 127.2, 125.8, 124.6, 120.2, 119.9, 115.9, 99.9, 68.1, 31.5, 29.2, 25.7, 22.5, 14.4. MALDI-TOF (m/z): 890.7 [M^+].

Acknowledgments

This work was supported by NSFC 9133316, 21403211, and "Chutian" project of China Three Gorges University. The authors thank the National Supercomputing Center in Shenzhen for providing computing resources.

References

1 A. Hagfeldt, G. Boschloo, L. Sun, L. Kloo and H. Pettersson, *Chem. Rev*., 2010, **110**, 6595-6663.
2 A. Hagfeldt and M. Graetzel, *Chem. Rev*., 1995, **95**, 49-68.
3 B. O'Regan and M. Gratzel, *Nature*, 1991, **353**, 737-740.
4 M. T. Spitler and B. A. Parkinson, *Acc. Chem. Res.,* 2009, **42**, 2017-2029.
5 S. Mathew, A. Yella, P. Gao, R. Humphry-Baker, B. F. Curchod, N. Ashari-Astani, I. Tavernelli, U. Rothlisberger, M. K. Nazeeruddin and M. Gratzel, *Nat. Chem.,* 2014, **6**, 242-247.
6 D. Shi, N. Pootrakulchote, R. Li, J. Guo, Y. Wang, S. M. Zakeeruddin, M. Grätzel and P. Wang, *J. Phys. Chem. C*, 2008, **112**, 17046-17050.
7 M. Gratzel, *J. Photoch. Photobio. A*, 2004, **164**, 3-14.

8 M. K. Nazeeruddin, A. Kay, I. Rodicio, R. Humphrybaker, E. Muller, P. Liska, N. Vlachopoulos and M. Gratzel, *J. Am. Chem. Soc.*, 1993, **115**, 6382-6390.
9 M. K. Nazeeruddin, P. Pechy, T. Renouard, S. M. Zakeeruddin, R. Humphry-Baker, P. Comte, P. Liska, L. Cevey, E. Costa, V. Shklover, L. Spiccia, G. B. Deacon, C. A. Bignozzi and M. Gratzel, *J. Am. Chem. Soc.*, 2001, **123**, 1613-1624.
10 Y. Chiba, A. Islam, Y. Watanabe, R. Komiya, N. Koide and L. Y. Han, *Jpn. J. Appl. Phys.*, 2006, **45**, L638-L640.
11 M. K. Nazeeruddin, P. Pechy and M. Gratzel, *Chem. Commun.*, 1997, 1705-1706.
12 A. Yella, H.-W. Lee, H. N. Tsao, C. Yi, A. K. Chandiran, M. K. Nazeeruddin, E. W.-G. Diau, C.-Y. Yeh, S. M. Zakeeruddin and M. Grätzel, *Science*, 2011, **334**, 629-634.
13 R. Li, J. Liu, N. Cai, M. Zhang and P. Wang, *J. Phys. Chem. B*, 2010, **114**, 4461-4464.
14 M. F. Xu, D. F. Zhou, N. Cai, J. Y. Liu, R. Z. Li and P. Wang, *Energ. Environ. Sci.*, 2011, **4**, 4735-4742.
15 W. Zeng, Y. Cao, Y. Bai, Y. Wang, Y. Shi, M. Zhang, F. Wang, C. Pan and P. Wang, *Chem. Mater.*, 2010, **22**, 1915-1925.
16 X. Jiang, K. M. Karlsson, E. Gabrielsson, E. M. J. Johansson, M. Quintana, M. Karlsson, L. Sun, G. Boschloo and A. Hagfeldt, *Adv. Funct. Mater.*, 2011, **21**, 2944-2952.
17 D. P. Hagberg, X. Jiang, E. Gabrielsson, M. Linder, T. Marinado, T. Brinck, A. Hagfeldt and L. Sun, *J. Mater. Chem.*, 2009, **19**, 7232-7238.
18 N. Robertson, *Angew. Chem. Int. Ed.*, 2006, **45**, 7321-7321.
19 A. Mishra, M. K. Fischer and P. Bauerle, *Angew. Chem. Int. Ed.*, 2009, **48**, 2474-2499.
20 H.-H. Chou, Y.-C. Chen, H.-J. Huang, T.-H. Lee, J. T. Lin, C. Tsai and K. Chen, *J. Mater. Chem.*, 2012, **22**, 10929.
21 G. Li, K. J. Jiang, Y. F. Li, S. L. Li and L. M. Yang, *J. Phys. Chem. C*, 2008, **112**, 11591-11599.
22 W. H. Liu, I. C. Wu, C. H. Lai, P. T. Chou, Y. T. Li, C. L. Chen, Y. Y. Hsu and Y. Chi, *Chem. Commun.,* 2008, 5152-5154.
23 C. J. Qin, A. Islam and L. Y. Han, *J. Mater. Chem. A,* 2012, **22**, 19236-19243.
24 R. Z. Li, X. J. Lv, D. Shi, D. F. Zhou, Y. M. Cheng, G. L. Zhang and P. Wang, *J. Phys. Chem. C*, 2009, **113**, 7469-7479.
25 J. Y. Liu, J. Zhang, M. F. Xu, D. F. Zhou, X. Y. Jing and P. Wang, *Energ. Environ. Sci.*, 2011, **4**, 3021-3029.
26 J. Y. Liu, D. F. Zhou, M. F. Xu, X. Y. Jing and P. Wang, *Energ. Environ. Sci.*, 2011, **4**, 3545-3551.
27 S. Y. Qu, C. J. Qin, A. Islam, Y. Z. Wu, W. H. Zhu, J. L. Hua, H. Tian and L. Y. Han, *Chem. Commun.*, 2012, **48**, 6972-6974.
28 Y. Z. Wu, M. Marszalek, S. M. Zakeeruddin, Q. Zhang, H. Tian, M. Gratzel and W. H. Zhu, *Energ. Environ. Sci.*, 2012, **5**, 8261-8272.
29 W. Zhu, Y. Wu, S. Wang, W. Li, X. Li, J. Chen, Z.-s. Wang and H. Tian, *Adv. Funct. Mater.*, 2011, **21**, 756-763.
30 S. Haid, M. Marszalek, A. Mishra, M. Wielopolski, J. Teuscher, J.-E. Moser, R. Humphry-Baker, S. M. Zakeeruddin, M. Grätzel and P. Bäuerle, *Adv. Funct. Mater.*, 2012, **22**, 1291-1302.
31 J. N. Clifford, E. Palomares, M. K. Nazeeruddin, M. Grätzel, J. Nelson, X. Li, N. J. Long and J. R. Durrant, *J. Am. Chem. Soc.*, 2004, **126**, 5225-5233.
32 F. De Angelis, G. Vitillaro, L. Kavan, M. K. Nazeeruddin and M. Grätzel, *J. Phys. Chem. C,* 2012, **116**, 18124-18131.
33 A. D. Becke, *J. Chem. Phys.,* 1993, **98**, 5648-5652.
34 B. J. Lynch, P. L. Fast, M. Harris & D. G. Truhlar, *J. Phys. Chem. A,* 2000, **104**, 4811-4815.
35 M. J. Frisch, G. W. Trucks, H. B. Schlegel, G. E. Scuseria, M. A. Robb, J.R. Cheeseman, *Gaussian 09: Revision A01*; 2009.
36 C. Longo, A. F. Nogueira, M. A. De Paoli, H. Cachet, *J. Phys. Chem. B,* 2002, **106**, 5925-5930.
37 F. Fabregat-Santiago, J. Bisquert, G. Garcia-Belmonte, G. Boschloo, A. Hagfeldt, *Sol. Energ. Mat. Sol. C,* 2005, **87**, 117-131.
38 J. Bisquert, F. Fabregat-Santiago, I. Mora-Sero, G. Garcia-Belmonte, S. Gimenez, *J. Phys. Chem. C*, 2009, **113**, 17278–17290.
39 R. Kern, R. Sastrawan, J. Ferber, R. Stangl, J. Luther, *Electrochim. Acta.,* 2002, **47**, 4213-4225.

Table of Contents

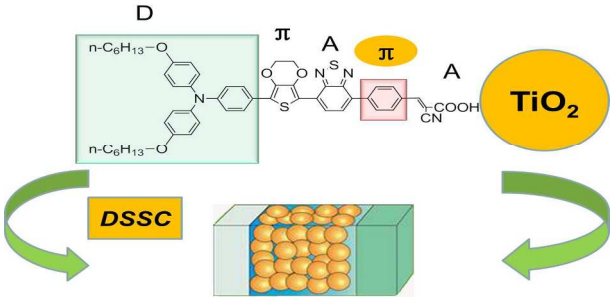

We proposed and synthesized a novel D–π–A–π–A type dye (C321) and demonstrated its application in dye-sensitized solar cells.